Electronic and optical properties of alkali-metal-intercalated single-wall carbon nanotubes

X. Liu,[1] T. Pichler,[1,2] M. Knupfer,[1] and J. Fink[1]
[1]*Leibniz-Institute for Solid State and Materials Research Dresden, P.O. Box 270016, D-01171 Dresden, Germany*
[2]*Institut für Materialphysik, Universität Wien, Strudlhofgasse 4, A-1090 Wien, Austria*
(Received 17 October 2002; published 5 March 2003)

We present recent studies of the structural and electronic properties of alkali-metal intercalated single-wall carbon nanotubes using high-resolution electron energy-loss spectroscopy (EELS) in transmission. Changes in the nanotube structure and electronic properties due to intercalation were monitored by *in situ* EELS measurement. The modulation of the nanotube bundle structure is reflected by the variations of the diffraction patterns. The core-level excitations show that there is no hybridization between nanotube π^* states and metal valence states. The intensity of the interband transitions is dramatically affected, demonstrating the possibility of tuning the Fermi level to specific bands upon intercalation. The charge carrier plasmon depends on both the intercalation level and the alkali metal. The loss function was analyzed using a Drude-Lorentz model to obtain more information about the optical properties.

DOI: 10.1103/PhysRevB.67.125403 PACS number(s): 73.22.−f, 78.67.Ch

I. INTRODUCTION

Since the discovery of carbon nanotubes,[1] a lot of attention has been focused on this new class of nanoscale materials, which are found as multiwall or single-wall carbon nanotubes (SWCNT's). Due to their unusual geometry, their structural and electronic properties, these carbon nanostructures are regarded as promising building blocks for molecular electronics.[2] Multiwall carbon nanotubes consist of several cylinders of bent graphite layers with a variety of electronic properties. In contrast, SWCNT's consist of a single graphene sheet rolled into a cylinder with diameters in the range of 1–2 nm and lengths of several hundred micrometers. Many studies have focused on the intriguing electronic properties of those novel quasi-one-dimensional structures. Calculations show that their electronic properties can be either semiconducting or metallic depending on their geometrical structure defined by the chirality.[3,4] These properties were experimentally proven by the combination of scanning tunneling microscopy and scanning tunneling spectroscopy.[5] The existence of semiconducting SWCNT's opens up the wide opportunity for nanoscale device applications.[6] Since in all semiconductor applications the properties of a device depend on the electronic states in the valence and the conduction bands, the control of the states in these bands is crucial to design and to optimize those devices. So, the future application of SWCNT's will depend upon the ability to modify their intrinsic properties by manipulation of their electronic structure.

One route for modifying the solid state properties of SWCNT's is the addition of electron acceptors or donors[7–10] or by electrochemical doping.[11–13] Both methods change the solid state properties drastically. It was shown that the Fermi level can be shifted by electron or hole doping. The doping can result in a significantly reduced electrical resistivity and work function. Furthermore, the electrochemical reactivity and the porosity make SWCNT bundles attractive host material for energy storage. The experiment shows that lithium intercalated SWCNT's have a remarkably high reversible lithium storage capacity.[14] The maximal intercalation for potassium doping has been found to be a C/K ratio of ≈ 7.[9] This value is similar to highest doping in graphite intercalation compounds (GIC KC_8)[15,16] and fullerenes intercalation compounds (FIC) (K_6C_{60}).[17]

In a bulk sample, most of the SWCNT's form long crystalline bundles, these bundles normally consist of a few tubes to thousands of tubes packed in a hexagonal lattice.[18,19] The nanotubes are kept together by van der Waals interactions with a typical interlayer spacing similar to that of graphite. The interstitial space of the tube bundles and the interior cavity can harbor intercalants through physisorption or chemisorption. In contrast to GIC and FIC this interstitial space is not as well defined because of the disorder of the SWCNT bundle lattice and the different chirality of the individual SWCNT's. Nevertheless the structural analysis of those intercalated SWCNT material can help to clarify some theoretical predictions. The issue of the structures of potassium intercalated SWCNT bundles has been approached by different theoretical arguments. For example, it has been predicted that the intercalated atoms are located at the interstitial sites of the tube bundles, but with the same tube spacing to be maintained after the intercalation, whereas the tube walls are severely distorted at an intercalation level of KC_{10}.[20] However, other results indicate that the intercalation can expand the lattice of the bundle, and predicted no distortion of the nanotube wall up to an intercalation level of KC_4.[21] In summary, the addition of intercalants to SWCNT's can be regarded as an important method to engineer the SWCNT's properties, and intercalation provides one way to modify their properties in a controlled way.

In this contribution, we present studies of the electronic structure of alkali-metal intercalated SWCNT's, i.e., sodium, potassium, rubidium, and cesium intercalation. The structural changes and the variation of the electronic properties were characterized by electron energy-loss spectroscopy (EELS) in transmission. The intercalation causes an expansion of the intertube distance. The analysis of the C 1*s* core-level excitations shows that there is no hybridization between

SWCNT's and the intercalants. The electrons that are transferred from the alkali metals to SWCNT's can fill the lower energy bands of the SWCNT's and give rise to the appearance of a free carrier plasmon in the intercalated SWCNT's, which shows intercalation level and intercalant dependence. Furthermore, the loss function was analyzed by an effective Drude-Lorentz model, and the optical conductivity has been derived from this model.

II. EXPERIMENTAL

SWCNT's used for our studies were produced by laser ablation.[22,23] The diameter of the SWCNT's is about 1.37 ± 0.05 nm as determined by electron and x-ray diffraction as well as optical absorption spectroscopy. Thin films with an effective thickness of about 100 nm were prepared by dropping an acetone suspension of SWCNT's onto KBr single crystals. After the KBr was dissolved in distilled water, the films were transferred to a standard 200 mesh platinum electron microscopy grid and heated to 770 K for several hours in ultrahigh vacuum to remove the organic contaminations in the films. The intercalation was carried out in an ultrahigh vacuum chamber by evaporation of alkali metals from commercial SAES getter sources. During alkali metal evaporation, the SWCNT film was kept at 420 K, together with a 20 min post anneal at the same temperature to improve intercalant homogeneity and remove excessive alkali metals from the film surface. This process was repeated several times until maximal intercalation was reached as revealed by a saturation in all characteristic changes discussed in this paper below. Subsequently, the intercalated SWCNT films were transferred into the measurement chamber (base pressure 1×10^{-10} mbar) of the purpose-built 170 keV EELS spectrometer[24] with the energy and momentum resolution being 180 meV and 0.03 Å^{-1} for the low energy-loss function and electron diffraction, respectively. For the C $1s$ excitation measurements the same energy resolution but a slightly reduced momentum resolution of 0.1 Å^{-1} was chosen. The loss function $\text{Im}[-1/\epsilon(\mathbf{q},\omega)]$, which is proportional to the dynamic structure factor $S(\mathbf{q},\omega)$, has been measured for various momentum transfers q. All measurements are performed at room temperature.

III. RESULTS AND DISCUSSION

A. Electron diffraction

During the SWCNT formation process van der Waals forces lead to the creation of bundles of SWCNT's in which the individual nanotubes are arranged within a hexagonal lattice. These bundles usually consist of SWCNT's with a finite diameter distribution.[25] X ray and electron diffraction are effective tools to investigate this lattice structure and provide information upon the mean diameter of the SWCNT's,[25–27] as the intertube distance is mainly dependent on the nanotube diameter. Within the SWCNT bundles, the interstitial channels between the tubes provide additional sites for intercalation. For nanotubes with a mean diameter of about 1.37 nm, the space in the bundle lattice is about 6 Å without including van der Waals radius, which is big enough as compared to the ion radii to harbor alkali metals. SWCNT bundles can be intercalated, though the exact position of the intercalated atoms in the bulk SWCNT bundles is still unknown. For an isolated SWCNT, binding sites of intercalants are located at the external surface of the tube through physisorption or chemisorption, and presumably in the interior of the tube if its ends are open. In the SWCNT's bundle, it is considered that the intercalated atoms are located at the interstitial channel sites and have a symmetric configuration so as to maximize the interatomic distance.[21] It is a natural idea that the insertion of the intercalated atoms into the bundle will enlarge the intertube distance, and the bigger the intercalated atoms are, the stronger this expansion effect is. First, we carried out a structural analysis using electron diffraction in the EELS spectrometer by setting the energy loss to zero, which gave results consistent with those of x-ray diffraction studies.[18]

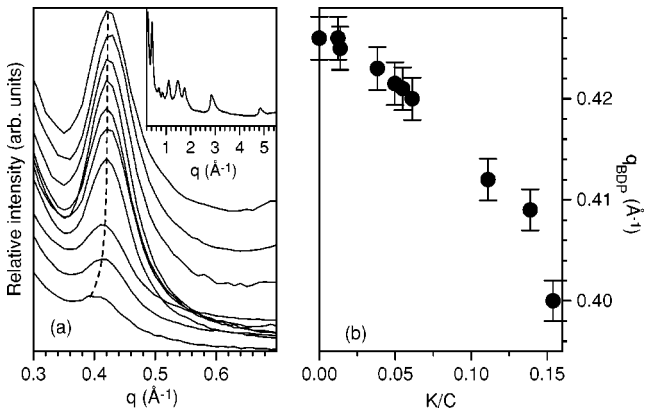

FIG. 1. (a) The variation of the first bundle diffraction peak with increasing potassium intercalation levels (from top to bottom), the inset shows the diffraction pattern of pristine SWCNT's in a wide q region. (b) The relation between the momentum transfer of the bundle diffraction peak position (q_{BDP}) and the relative atom ratio between potassium and carbon.

In the inset of Fig. 1(a) the electron diffraction pattern of pristine SWCNT's is shown. The lower q part corresponds to bundle diffraction and the higher q part is ascribed to the contribution of the roll-up graphene sheet. The effect of intercalation will be reflected by changes of the bundle diffraction pattern. Here we focus on the first bundle peak only which appears with highest intensity. Figure 1(a) shows the raw electron diffraction data of the first bundle peak from pristine and potassium-intercalated SWCNT's samples as a function of the potassium content. It is clearly seen that with the increase of potassium concentration, the bundle diffraction peak shifts to lower q and the intensity decreases.[9] The downshift of the bundle peak stands for an increase of the intertube distance. This is consistent with an expansion of the internanotube spacing concomitant with intercalation in between the SWNCT's in the bundles. In the present sample, the downshift is from 0.426 to about 0.4 Å^{-1} for the fully potassium intercalated material, which corresponds to the variation of the intertube distance from about 1.7 nm (pristine) to 1.81 nm (fully intercalated). The extent of bundle expansion is a little smaller than the ion radius of potassium, which is about 1.38 Å.

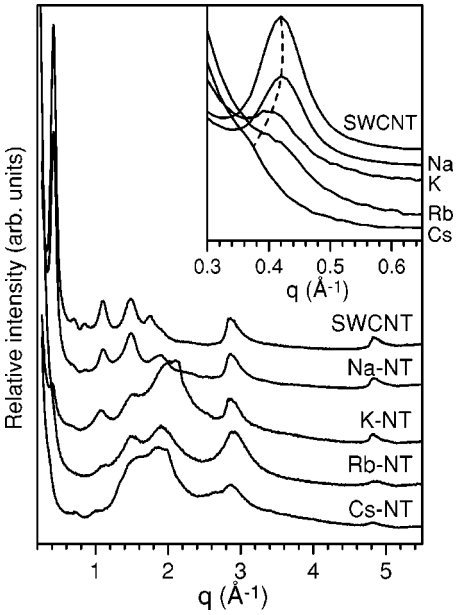

FIG. 2. The electron diffraction patterns of pristine SWCNT's and fully sodium, potassium, rubidium, and cesium-intercalated SWCNT's. The inset shows the first bundle peak, the dashed line indicates the downshift of bundle peak due to different intercalants.

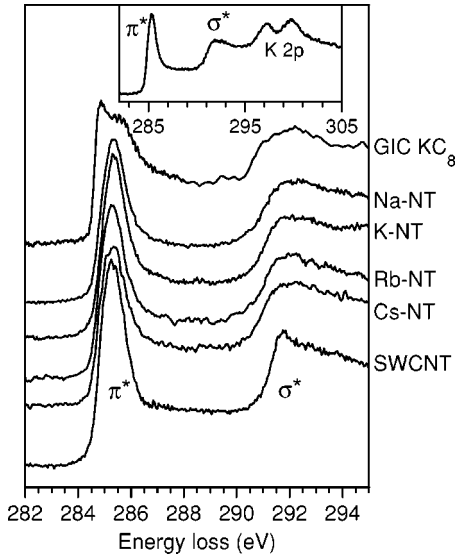

FIG. 3. Core-level excitations of pristine and fully sodium, potassium, rubidium, and cesium-intercalated SWCNT's, respectively. The C 1*s* of graphite intercalated compounds KC_8 is shown at the top for comparison. The inset shows the C 1*s* spectrum of potassium-intercalated SWCNT's in wide range.

The intensity decrease of the bundle peak mostly results from the insertion of intercalants into the bundle which also will cause more disorder and thus a decrease of the respective Bragg peak intensity. Furthermore, Fig. 1(b) depicts the relation between bundle peak and the K concentration quantitatively, where the potassium concentrations can be estimated from C 1*s* and K 2*p* core-level excitations (see below). An almost linear decrease of the peak position is observed.

Next we turn to the electron diffraction of SWCNT films intercalated with other alkali metals, such as sodium, rubidium and cesium, as shown in Fig. 2. It is clearly shown that the intensity of the first Bragg peak becomes weaker and weaker from sodium to cesium intercalation. The bigger the size of the intercalant, the lower the intensity in the Bragg peak. Furthermore, the position of the first Bragg peak shifts to lower q with increasing alkali ionic radius. For sodium intercalation, the position change of the first bundle peak is very weak as compared to pristine SWCNT's. This can be ascribed to the smaller diameter of sodium ions and the relatively large space within SWCNT bundles in the present sample with a mean diameter of about 1.37 nm, where the intertube space is big enough to incorporate sodium ions with a radius of about 0.95 Å without any significant expansion effect of the nanotube bundles. As a test, SWCNT films with a smaller diameter (about 1.07 nm) were intercalated with sodium and a clear downshift of the first Bragg peak occurred, which corresponds to the increase of the intertube distance from about 1.42 to 1.54 nm (data not shown here). In the inset of Fig. 2, the diffraction pattern of the first bundle peak of the fully intercalated SWCNT films is plotted in an enlarged range for different intercalants. The intertube distance can be estimated assuming the triangular lattice structure of bundles still kept, for rubidium and cesium intercalation, the increase of the intertube distance is 1.7 and 2.7 Å, respectively, which is consistent with the larger ionic radii of rubidium and cesium of 1.48 and 1.69 Å, respectively. Furthermore, additional diffraction intensity for K, Rb, and Cs intercalation is observed below 2.2 Å^{-1}. The center of this additional intensity shifts downward going to the heavier alkalis. This observation can probably be attributed to electron diffraction by the intercalants which form quasi-one-dimensional chains inbetween the nanotubes. The downshift might be ascribed to the increase of the ionic radii which gives rise to a growing alkali-alkali distance going from K to Cs.

B. Core-level excitations

Information on the electronic structure of intercalated SWCNT's can be extracted from the analysis of the core-level excitations from the C 1*s* level. The electron excitations of carbon C 1*s* core electrons into empty π^* orbitals are probed. C 1*s* core-level EELS spectra are measured at small q and in this high-energy region $\mathrm{Im}(-1/\epsilon) \approx \epsilon_2$; hence the measured core edge structure corresponds directly to electronic C 1*s* transitions into unoccupied states with C 2*p*-related (unoccupied) $\pi^\star$ and $\sigma^\star$ character. The former is characterized by a nearly symmetric peak centered at around 285.4 eV, while the latter starts at around 292 eV. These energies closely resemble those observed for the analogous excitations in graphite,[28] while the SWCNT spectrum is similar to an average of the in-plane and out-of-plane graphite spectra.[29] For intercalation, the C 1*s* spectra of the intercalated SWCNT's are shown in Fig. 3, where the different alkali-metal intercalations at the maximal intercalation level are depicted together. For comparison, C 1*s* core-level excitations of the pristine SWCNT's and the GIC KC_8 are also shown in Fig. 3. From the figure it can be seen that the shape

of all spectra of the intercalated SWCNT's is virtually identical in the energy range between 280 and 295 eV. In the higher energy range as shown in the inset of Fig. 3, K $2p$ excitations are present in potassium intercalated SWCNT's. The potassium concentration can be obtained from the relative intensity ratio of K 2p/C $1s$ core-level excitations signals.[9] For the K/C calibration, we first normalize to the inflection point of the $\sigma^\star$ onset. The spectral weight from the K $2p$ core level excitations is then determined by subtraction of the pristine spectrum in each case, whereby, the K/C ratios for the GIC KC_8 is well known from structural measurement and taken as reference. For K intercalation, a maximal C/K ratio of about 6.5 is observed. The two excitonic transitions (into $\pi^\star$ and $\sigma^\star$ states) in pristine SWCNT's (Ref. 29) are only little affected by the alkali-metal intercalation, their line shape and their positions remain unchanged.

It is interesting to compare the C $1s$ spectra of the intercalated SWCNT's with those of alkali-metal GIC,[30] as shown in Fig. 3. It can be clearly seen that the spectral shape above the excitation onset is identical for all doped SWCNT's exhibiting only a single narrow peak at 285.4 eV very similar to GIC KC_{24}.[30] However, in the alkali-metal GIC KC_8 the C $1s$ spectrum shows a double-peaked structure. This can be ascribed to hybridization of the $\pi^\star$ and metal states above the Fermi level.[30] On the other hand, the identical structure of pristine and alkali-metal intercalated SWCNT's suggests that there is no hybridization between SWCNT $\pi^\star$ states and metal valence states, which may be related to the curvature of the graphene sheets in SWCNT's.

The predicted singularities in the unoccupied C $2p$-derived electronic density of states of the SWCNT's are conspicuous by their absence in the C $1s$ excitation spectra due to the effect of the C $1s$ core hole in the final state. In the case of C $1s$ excitations of graphite, both the $\pi^\star$ and $\sigma^\star$ onsets are dominated by spectral weight resulting from the influence of the core hole.[31,32] Thus, assuming a similar interaction between the excited electron and the core hole in SWCNT's, we can expect that the $\pi^\star$ resonances related to the density of states singularities of the different types of SWCNT's are washed out, resulting in the broad peak centered at 285.4 eV. Although there is a shift of the Fermi level to the conduction band in intercalated SWCNT's, this strong excitonic effect renders it invisible in the C $1s$ core-level excitation spectrum. The amount of charge transfer from the alkali metal ions to the SWCNT conduction band can be estimated from an analysis of the spectral weight of the $\pi^\star$ feature. For all fully intercalated SWCNT's, it reveals a decrease of about 10% as compared to pristine nanotubes. This decrease is in good agreement with a complete charge transfer from the outer alkali s electrons to the nanotubes. It yields an intercalation ratio for maximally intercalated SWCNT's of around $C/A \approx 10$ (A = alkali metal) for all alkali metals which is in good agreement with the above mentioned structural observations.

C. Optical response

Calculations show that SWCNT's can be either semiconducting or metallic depending on the chirality, and their band gap is inversely proportional to their diameter. The investigated films contain a distribution of tube diameters and chiralities such that the experimental signal is in fact averaged and hence broadened in energy. For example, in the optical absorption spectra of the pristine films several features are visible.[22,23] The strongest peaks correspond to excitation energies around 0.7, 1.2 and 1.8 eV for nanotubes with a mean diameter of about 1.4 nm. All these features are superimposed to a broad absorption band located at roughly 4.5 eV (related to the π-$\pi^\star$ interband transitions). The first two absorption bands can be assigned to the first two interband transitions between the van Hove singularities in the electronic density of states of the semiconducting SWCNT's. The transition at around 1.8 eV corresponds to the first set of singularities in the density of states of the metallic nanotubes. Experimentally, it has been demonstrated that, similar to optical absorption spectroscopy,[22,23] EELS in transmission is a very powerful tool to study the optical properties of bulk samples of SWCNT's, also as a function of momentum transfer.[33] EELS in transmission using low momentum transfers probes the optical limit, thus the low-energy peaks in the loss function are due to collective excitations caused by the optically allowed transitions.[33] From the spectra due to these optically allowed transitions in EELS measurement, the changes of the related electronic states due to intercalation can be studied. The disappearance of structures in the spectra can thus be interpreted as due to a filling of unoccupied states with electrons from the alkali metals.[10] Additional features might also arise during the intercalation process, which then can be assigned to new, intercalation-induced interband excitations or a charge carrier (Drude) plasmon, respectively.[9]

1. Doping dependence of the electronic excitations of potassium intercalated SWCNT's

We now turn our attention to the modulation of the interband transitions of SWCNT's by intercalation with potassium. As discussed above, for each K donor the outer $4s$ electrons will be transferred to the SWCNT's. The transferred charge will fill states of the conduction band of SWCNT's and result in a Fermi level shift to higher energies. This is revealed by low energy loss function measurements. Figure 4(a) shows the raw data of the evolution of the loss function upon potassium intercalation starting with pristine SWCNT's from the bottom in a energy range between 0.2 and 9 eV at $q = 0.1$ Å^{-1}. The wide peak at around 6 eV is the π plasmon related to a collective excitation of π electrons in SWCNT's,[33] while the three loss function peaks in the pristine nanotubes below 3.0 eV stem from the abovementioned optically allowed interband transitions. The evolution of the loss function shows an intensity decrease of the lowest interband transitions with increasing potassium concentration. It can be clearly seen that the change in intensity of these interband transition peaks in EELS depends sensitively on the amount of the intercalant. With increase of potassium concentration, it is shown that the three interband transitions finally disappear [see the spectrum for C/K = 26 in Fig. 4(a)] in good agreement with optical observations.[10] This can be straightforwardly interpreted via a charge trans-

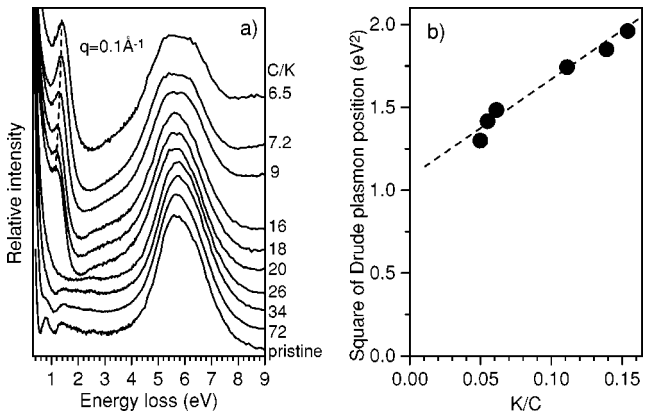

FIG. 4. (a) The loss function of pristine SWCNT's and potassium-intercalated SWCNT's with different intercalation levels at $q=0.1$ Å^{-1}, the potassium concentration increases from bottom to top as marked on the right side. The dashed line indicates the shift of the position of the charge carrier plasmons with increasing potassium concentration. (b) The quantitative relation between the square of the energy position of the charge carrier plasmon and the relative potassium concentration.

fer within the framework of a rigid-band model. In the case of alkali-metal intercalation the conduction bands are populated with electrons. Consequently, some previously allowed optical transitions are suppressed as their final states become occupied. Gradual filling of the empty states within the density of the states first quenches the lowest energy transitions, while the higher energy transitions are not affected initially. For higher intercalation levels, electronic final states of the second transition of semiconductiong SWCNT's are filled such that the transition at the second lowest energy vanishes. In the present study, the intercalation for this stage roughly is C/K $\approx$26. Up to this intercalation stage, the shape of the loss function at higher energies is kept unchanged in comparison with that of pristine nanotubes.

With further increase of the potassium intercalation level an additional peak occurs in the loss function in the energy range between 1 and 2 eV. Its energy position shifts to higher values with increasing intercalation. Therefore, an origin of this peak due to interband transitions can be ruled out because its energy position then would be roughly independent upon intercalation. The new feature in contrast can be associated with the collective excitation of the introduced conduction electrons, the so-called charge carrier or Drude plasmon.[9] As can be seen in Fig. 4(a), it reaches about 1.4 eV at maximal doping. The upshift of this plasmon with increasing intercalation level is consistent with the increase of the density of charge carriers. In Fig. 4(b), the square of the charge carrier plasmon energy dependence on the potassium concentration which was estimated from the relative intensity ratio of K $2p$ and C $1s$ core-level excitations is shown. Within the simplest approximation, the Drude plasmon energy $E_{p,D}$ should have a square root dependence upon the charge carrier density n. From Fig. 4(b), it is obvious that there is such a linear dependence of $E_{p,D}^2$ on the K concentration. However, it is not possible to model the observed plasmon positions using the relation $E_{p,D}^2 = \hbar^2 ne^2/(m^\star \epsilon_\infty \epsilon_0)$ ($m^\star$ = charge carrier effective mass, ϵ_∞ = background dielectric constant).[34] Since the results of the C $1s$ core level studies above indicate a full charge transfer, i.e., a charge carrier density n, which is proportional to the intercalation level, Fig. 4(b) indicates that the product $m^\star \epsilon_\infty$ in the denominator is not constant as a function of intercalation.

TABLE I. Parameters for the Drude (D) plasmon in eV from the simulation of the loss function of GIC KC_8, and the K intercalated SWCNT's with stoichiometry as indicated.

	Drude				
	$E_{p,0}$	Γ_0	ϵ_∞	$\frac{m^\star}{m_0}$	σ_0 (S cm^{-1})
GIC KC_8	5.8	0.2	6.7	0.4	22625
C/K=20	3.4	0.7	6	0.4	2330
C/K=18	3.4	0.6	6.1	0.4	2450
C/K=16	3.5	0.6	6.1	0.5	2730
C/K=9	3.6	0.6	6.1	0.7	2780
C/K=7.2	3.8	0.7	6.1	0.8	2900
C/K=6.5	3.9	0.7	6.1	0.8	2940

In order to obtain more detailed information we analyze the measured loss function using a Drude-Lorentz model. The dielectric function of the intercalated SWCNT's can be expressed within a straightforward Drude-Lorentz model which was successfully applied to describe graphite or SWCNT intercalated compounds, and can be written as

$$\epsilon(E) = 1 - \frac{E_{p,0}^2}{E^2 - i\Gamma_0 E} + \sum \frac{E_{p,i}^2}{(E_{T,i}^2 - E^2) + i\Gamma_i E}, \quad (1)$$

where the first term is the contribution of the Drude plasmon with plasmon energy $E_{p,0}$ and its damping Γ_0, the second term is ascribed to the different Lorentz harmonic oscillators with the energy of the oscillators $E_{T,i}$, and the strength of the oscillator $E_{p,i}$ which can be expressed as $E_{p,i} bf = \hbar \cdot \sqrt{n_i e^2/(\epsilon_0 m^\star)}$ with n_i being the density of electrons that contribute to the oscillator and $m^\star$ being their effective mass. Γ_i describes the damping of the oscillator. In the case of intercalated SWCNT's, the fit will include a charge carrier plasmon, one interband oscillator giving rise to the π plasmon and another oscillator for the $\pi+\sigma$ plasmon. Furthermore, since the π and $\pi+\sigma$ plasmon screen the Drude plasmon which leads to a shift to lower energies, their contribution at low energies can be expressed using a constant dielectric background ϵ_∞. In order to determine ϵ_∞, the loss function is modelled with the abovementioned two Lorentz oscillators and their contribution to the real part of the dielectric function at the Drude plasmon energy is taken as ϵ_∞. Subsequently, the Drude plasmon is fitted using this dielectric background. The fit parameters are presented in Table I while the fitted curves are shown together with the data in Fig. 5. It turns out that the dielectric background ϵ_∞ is about 6.1 and almost independent of the intercalation level. We attribute this to the fact that intercalation does not result in a significant rearrangement of the majority of the π and

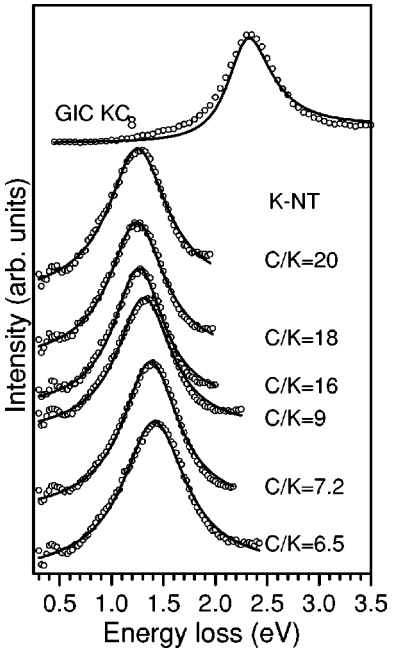

FIG. 5. Analysis of the loss function of potassium-intercalated SWCNT's after removing the quasielastic scattering background and compared with GIC KC_8. The solid line is fitted curve, and the open circle represents experimental data. The potassium stoichiometry is indicated.

$\pi+\sigma$ electronic states. Thus, considering $\epsilon_\infty=6.1$ and change in the charge carrier density which is proportional to the intercalation level one arrives at an effective mass of the charge carriers $m^\star$ in the range of 0.37–0.82 times that of the free electron mass m_0, whereas $m^\star$ is increasing upon increasing intercalation.[35] The corresponding values are also shown in Table I. The obtained optical effective mass for GIC KC_8 in our experiment is consistent with the effective mass from the optical measurement[16,36] but it is a littler lower compared with the value from de Hass–van Alphen experiments.[37] For the intercalated SWCNT's, the increase of the effective mass with intercalation might be related to the upshift of the Fermi level to an energy region where the conduction bands become flatter.

Finally, the prominent feature at 6 eV in Fig. 4(a) which is assigned to the plasmon oscillation of all π electrons becomes broader and broader with growing intercalation level, while its energy position shifts only very little to lower energies. This is in contrast to GIC KC_8 where a downshift of the π plasmon from about 7 to 6.3 eV is observed.[30,38,39] It should be mentioned that the little downshift in the case of SWCNT's is diameter dependent, the smaller diameter of the SWCNT's the larger the downshift of the π plasmon upon alkali metal intercalation, but it is always very small compared to the downshift in intercalated graphite KC_8 which shows that, in general, the electronic levels of SWCNT's are little affected by the intercalation process.

2. Charge carrier plasmon dependence upon the intercalant

The appearance of a charge carrier plasmon at higher intercalation levels of SWCNT's is common to all alkali-metal intercalants. Figure 6(a) shows the loss function of fully sodium, potassium, rubidium, and cesium-intercalated SWCNT's compared with that of pristine nanotubes at a momentum transfer $q=0.1$ Å^{-1}. It is clearly seen that the charge carrier plasmon shifts to higher energies going from Na to Cs [as shown in Fig. 6(b)]. This is in contrast to GIC where for the alkali metals (Na, K, Rb, and Cs) the Drude plasmon is found at about 2.4 eV.[38] To shed more light on this behavior we again modeled the loss function as described above. The results are included in Table II. Upon increasing ion radius, there is a tendency to smaller values for the dielectric background. This might be related to the larger distance between the tubes as a results of intercalation (see discussion above). However, we note that alkali metal caused electronic excitations (e.g., excitations from K $3p$ into K $3d$ electronic levels) also contribute to the dielectric background, i.e., the screening of the charge carrier plasmon, and their contribution is not related to the ion radius as it sensitively depends upon the energy position and the spectral weight of the corresponding excitation. The unscreened plasma energy $E_{p,0}$ is about 3.4–3.8 eV almost independent of the alkali metals level which suggests that the bundle lattice expansion affects the plasma energy only little. As can be also seen from Table II, the effective mass of the charge

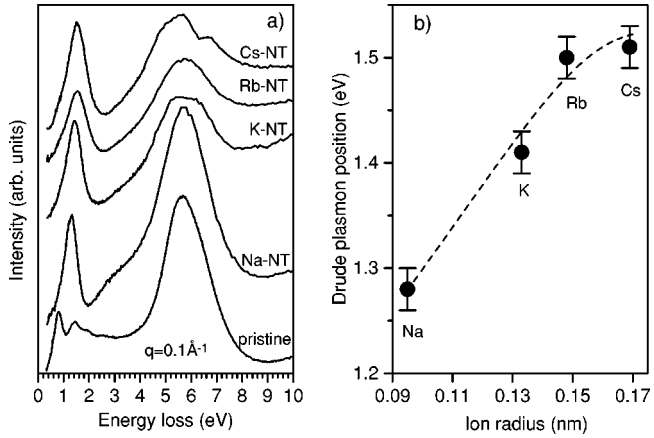

FIG. 6. (a) The loss function of pristine, fully sodium, potassium, rubidium, and cesium-intercalated SWCNT's at the energy range between 0 to 9 eV after background subtraction. (b) The dependence of the Drude plasmon position on the ion radius at the different alkali-metal intercalations.

TABLE II. Parameters for the Drude (D) plasmon in eV from the simulation of the loss function of GIC KC_8, fully Na, Rb, K, and Cs intercalated SWCNT's.

	Drude				
	$E_{p,0}$	Γ_0	ϵ_∞	$\frac{m^\star}{m_0}$	σ_0 (S cm^{-1})
GIC KC_8	5.8	0.2	6.7	0.4	22625
Cs-NT	3.6	0.9	4	0.8	1890
Rb-NT	3.8	1.0	4.7	0.7	1980
K-NT	3.9	0.7	6.1	0.8	2940
Na-NT	3.4	0.6	5.5	1.1	2470

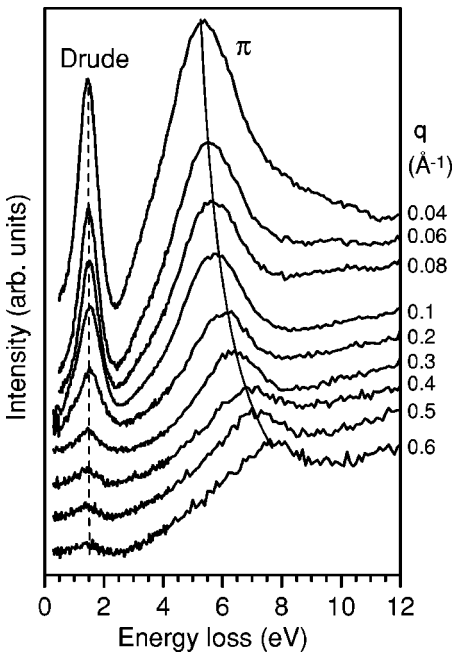

FIG. 7. The momentum dependence of the loss function in the fully rubidium-intercalated SWCNT's after subtracting the quasi-elastic scattering background. The dashed line indicates the Drude plasmon dispersion, the solid line depicts the π plasmon dispersion.

carriers is about 0.74–1.11 times that of the free electron mass for the fully intercalated SWCNT's. The scatter between the different intercalants might be related to the uncertainties concerning the exact intercalation level which is assumed to be the same for saturated intercalation independent of the intercalant.

There is again no clear shift of the position of π plasmon near 6 eV in all alkali-metal intercalated samples. Such a behavior is consistent with GIC with different intercalants.[30] However, as mentioned earlier, there is an obvious downshift of the π plasmon in GIC as compared to pristine graphite[30,38,39] which is not observed in the case of SWCNT's.

3. Drude plasmon dispersion

We have additionally studied the dispersion of the charge carrier plasmon. Since we observed no difference between the plasmon dispersions as a function of the intercalant, we show in Fig. 7 one representative example, the plasmon dispersion of the fully intercalated Rb sample in a momentum range of 0.04 to 0.6 $Å^{-1}$. The background due to the elastic line has been removed from the spectra in Fig. 7. As it is seen from the figure, there are two features in the loss function, the charge carrier plasmon and the π plasmon whose dispersion is radically different. The π plasmon disperses to higher energies with increasing momentum and the dispersion is very similar to that found for the π plasmon in pristine SWCNT's.[33] This again indicates that the electronic states of SWCNT are to a large extent only slightly affected by the intercalation process.

In contrast to the π plasmon, the charge carrier plasmon does not show a dispersion. Since the plasmon dispersion is proportional to the mean Fermi velocity, this indicates that the Fermi velocity of intercalated SWCNT is rather small, a conclusion which is consistent with the arguments above that in fully intercalated SWCNT's the Fermi level lies in a flat band region. Furthermore, with increasing momentum transfer the intensity of the charge carrier plasmon decreases very rapidly which renders it difficult to follow its energy position at higher momentum. The drastic decrease in intensity can be ascribed to a damping of the plasmon as a result of interband excitations between valence and conduction bands in intercalated SWCNT's (Landau damping).

4. Optical conductivity

From the Drude-Lorentz model analysis of the intercalated SWCNT's, additional information, e.g., about the optical conductivity can be extracted. Experimental and theoretical studies have shown that intercalation increases the conductivity of SWCNT mats significantly.[7] From the parameters in Tables I and II, the optical conductivity at zero energy can be obtained from the expression $\sigma_0 = E_p^2 \epsilon_0 / (\Gamma \hbar)$. The results show that the optical conductivity increases with higher intercalation level and its value is intercalant dependent. In particular, the larger intercalants, Rb and Cs, results in a lower conductivity which is directly related to the larger width of the charge carrier plasmon. This most probably is caused by a bigger structural disorder within the nanotube bundles as a consequence of the introduction of big ions and the corresponding expansion of the bundle lattice.

IV. SUMMARY

In summary, we have presented studies of the unoccupied electronic structure and the optical properties of alkali-metal intercalated SWCNT bundles using EELS in transmission. The intercalation can modify the bundle structure of SWCNT's. Compared with the spectra of the alkali-metal GIC, the core-level excitations of intercalated SWCNT's show that there is no hybridization between nanotube π^* states and metals valence states, and that states above the nanotube Fermi level remain rather unperturbed by the intercalant. Furthermore, the intercalation systematically modulates the optical response of SWCNT's. The measurements of the doping dependence show an intensity variation of the optical excitations due to the variation of the Fermi level position, indicating the possibility of tuning the Fermi level into conduction bands upon different electron donor intercalation. Upon intercalation the energy of the charge carrier plasmon increases at higher intercalation level and with the ion radius of the alkali metals. The density response function can be described within an effective Drude-Lorentz model, which allows the derivation of the optical conductivity at zero frequency σ_0 of sodium, potassium, rubidium, and cesium-intercalated SWCNT bundles. The results have been used to derive the dielectric background and the effective (optical) charge carrier mass of the intercalated SWCNT's which is found to be about two or three times bigger than in the corresponding GIC.

ACKNOWLEDGMENTS

We acknowledge financial support from the DFG (Grant Nos. FI 439/8-1 and PO 392/10-1), the SMWK (Grant No. 75 31.50-03-823-98/5), and the EU (IST Project SATURN). T.P. thanks the ÖAW for funding in form of an APART grant and the FWF P14146 for funding.

[1] S. Iijima, Nature (London) **354**, 56 (1991).
[2] C. Dekker, Phys. Today **52**, 22 (1999).
[3] N. Hamada, S. Sawada, and A. Oshiyama, Phys. Rev. Lett. **68**, 1579 (1992).
[4] R. Saito, G. Dresselhaus, and M.S. Dresselhaus, *Physical Properties of Carbon Nanotubes* (Imperial College Press, London 1998).
[5] J.W.G. Wildoer, L.C. Venema, A.G. Rinzler, R.E. Smalley, and C. Dekker, Nature (London) **391**, 59 (1998).
[6] T.W. Ebbesen, H.J. Lezec, H. Hiura, J.W. Bennett, H.F. Ghaemi, and T. Thio, Nature **382**, 54 (1996); S.J. Tans, M.H. Devoret, H. Dai, A. Thess, R.E. Smalley, L.J. Geerligs, and C. Dekker, *ibid.* **386**, 474 (1997).
[7] R. S. Lee, H.J. Kim, J.E. Fischer, A. Thess, and R.E. Smalley, Nature (London) **338**, 255 (1997).
[8] A.M. Rao, E. Richter, S. Bandow, B. Chase, P.C. Eklund, K.A. Williams, S. Fang, K.R. Subbaswamy, M. Menon, A. Thess, R.E. Smalley, G. Dresselhaus, and M.S. Dresselhaus, Science **275**, 187 (1997).
[9] T. Pichler, M. Sing, M. Knupfer, M.S. Golden, and J. Fink, Solid State Commun. **109**, 721 (1999).
[10] R. Jacquemin, S. Kazaoui, D. Yu, A. Hassanien, N. Minami, H. Kataura, and Y. Achiba, Synth. Met. **115**, 283 (2000); S. Kazaoui, N. Minami, R. Jacquimin, H. Kataura, and Y. Achiba, Phys. Rev. B **60**, 13 339 (1999).
[11] P. Petit, C. Mathis, C. Journet, and P. Bernier, Chem. Phys. Lett. **305**, 370 (1999).
[12] A. Claye, J.E. Fischer, and A. Metrot, Chem. Phys. Lett. **330**, 61 (2000).
[13] L. Kavan, P. Rapta, and L. Dunsch, Chem. Phys. Lett. **328**, 363 (2000).
[14] H. Shimoda, B. Gao X.P. Tang, A. Kleinhammes, L. Fleming, Y. Wu, and O. Zhou, Phys. Rev. Lett. **88**, 015502 (2002).
[15] M.S. Dresselhaus and G. Dresselhaus, Adv. Phys. **30**, 139 (1981).
[16] J.E. Fischer, J.M. Bloch, C.C. Shieh, M.E. Preil, and K. Jelley, Phys. Rev. B **31**, 4773 (1985).
[17] O. Zhou, J.E. Fischer, N. Coustel, S. Kycia, and Q. Zhu, Nature (London) **351**, 462 (1991).
[18] A. Thess, R. Lee, P. Nikolaev, H. Dai, P. Petit, J. Robert, C.H. Xu, Y.H. Lee, S.G. Kim, A.G. Rinzler, D.T. Colbert, G.E. Scuseria, D. Tomanek, J.E. Fischer, and R.E. Smalley, Science **273**, 483 (1996).
[19] A.G. Rinzler, J. Liu, H. Dai, C.B. Huffman, F. Rodriguez-Macias, P.J. Boul, A.H. Lu, D. Heymann, D.T. Colbert, R.S. Lee, J.E. Fischer, A.M. Rao, P.C. Eklund, and R.E. Smalley, Appl. Phys. A: Mater. Sci. Process. **67**, 29 (1998).
[20] G. Gao, T. Cagin, and W.A. Goddard III, Phys. Rev. Lett. **80**, 5556 (1998).
[21] C. Jo, C. Kim, and Y.H. Lee, Phys. Rev. B **65**, 035420 (2002).
[22] O. Jost, A.A. Gorbunov, W. Pompe, T. Pichler, R. Friedlein, M. Knupfer, M. Reibold, H.-D. Bauer, L. Dunsch, M.S. Golden, and J. Fink, Appl. Phys. Lett. **75**, 2217 (1999).
[23] H. Kataura, Y. Kumazawa, Y. Maniwa, I. Umezu, S. Suzuki, Y. Ohtsuka, and Y. Achiba, Synth. Met. **103**, 2555 (1999).
[24] J. Fink, Adv. Electron. Electron Phys. **75**, 121 (1989).
[25] D. Bernaerts, A. Zettl, N.G. Chopra, A. Thess, and R.E. Smalley, Solid State Commun. **105**, 145 (1998).
[26] H. Kuzmany, W. Plank, M. Hulman, Ch. Kramberger, A. Gruneis, Th. Pichler, H. Peterlik, H. Kataura, and Y. Achiba, Eur. Phys. J. B **22**, 307 (2001).
[27] J.M. Cowley, P. Nikolaev, A. Thess, and R.E. Smalley, Chem. Phys. Lett. **265**, 379 (1997); L. Henrard, P. Bernier, C. Journet, and A. Loiseau, Synth. Met. **103**, 2533 (1999).
[28] E.J. Mele and J.J. Ritsko, Phys. Rev. Lett. **43**, 68 (1979).
[29] M. Knupfer, Surf. Sci. Rep. **42**, 1 (2001).
[30] L.A. Grunes and J.J. Ritsko, Phys. Rev. B **28**, 3439 (1983).
[31] P.A. Brühwiler, A.J. Maxwell, C. Puglia, A. Nilsson, S. Andersson, and N. Mårtensson, Phys. Rev. Lett. **74**, 614 (1995).
[32] Y. Ma, P. Skytt, N. Wassdahl, P. Glans, D.C. Mancini, J. Guo, and J. Nordgren, Phys. Rev. Lett. **71**, 3725 (1993).
[33] T. Pichler, M. Knupfer, M.S. Golden, J. Fink, A.G. Rinzler, and R.E. Smalley, Phys. Rev. Lett. **80**, 4729 (1998).
[34] From A. Ugawa, A. Rinzler, and D.B. Tanner, Phys. Rev. B **60**, R1130 (1999), the Drude plasmon ($E_{p,D}$) of the pristine SWCNT's is only about 200 meV, its contribution to the charge carrier plasmons can be neglected.
[35] We use (10,10) to estimate the volume of the unit cell for calculating the electron density.
[36] G.L. Doll, M.H. Yang, and P.C. Eklund, Phys. Rev. B **35**, 9790 (1987).
[37] G. Wang, W.R. Datars, and P.K. Ummat, Phys. Rev. B **44**, 8294 (1991).
[38] J.J. Ritsko, Phys. Rev. B **25**, 642 (1982).
[39] D.M. Hwang, M. Ultraut, and S.A. Solin, Synth. Met. **3**, 81 (1981).